Implementation of active and passive loads alleviation methods on a generic mid-range aircraft configuration

Handojo, Vega; Lancelot, Paul; de Breuker, Roeland

DOI
10.2514/6.2018-3573

Publication date
2018

Document Version
Accepted author manuscript

Published in
2018 Multidisciplinary Analysis and Optimization Conference

Implementation of Active and Passive Loads Alleviation Methods on a Generic Mid-Range Aircraft Configuration

Vega Handojo*
DLR German Aerospace Center
Institute of Aeroelasticity, 37073 Göttingen, Germany

Paul Lancelot†, Roeland De Breuker‡
Delft University of Technology
Faculty of Aerospace Engineering, Delft, the Netherlands

Abstract: Loads analysis and structural design are core steps of the aircraft design process. To reduce wing loads and with it the wing structural mass, methods of passive and active loads alleviation have been researched in recent years. However, those methods are currently implemented without the consideration of dynamic simulations or unsteady aerodynamics in the optimization process in aircraft predesign. The purpose of this research is to investigate the influence of passive and active loads alleviation methods on the structural mass in aircraft preliminary design. The methods have been applied on the wing of a Generic Mid-Range (GMR) aircraft configuration. The models have been created with ModGen, an in-house program at DLR Institute of Aeroelasticity. The models comprise FE-models for the structure and masses, as well as DLM (Doublet-Lattice-Method) model for the aerodynamics. For the investigation of the influence of the loads alleviation systems, a loop of loads analysis and subsequent structure optimization has been conducted. The loads analysis consists of gust and maneuver simulations. For the passive loads alleviation, an aeroelastic tailoring of the wing structure has been implemented, whereas for the active loads alleviation the ailerons are deflected to redistribute lift during maneuvers and to partially compensate lift increment during gust encounters. With the implemented methods, a first quantification of the influence of loads alleviation methods on the structural mass in aircraft predesign is possible.

Nomenclature and abbreviations

c_z	=	lift increment
$c_{z\xi}$	=	lift increment due to aileron deflection
F_z	=	vertical shear force
M_x	=	bending moment
M_y	=	torque
ξ	=	aileron deflection
V_C	=	maximum operating speed
V_D	=	design dive speed

GLA:	Gust Loads alleviation
GMR:	Generic Mid-Range
HTP:	horizontal tailplane
MLA:	Maneuver Loads alleviation
ModGen:	Model Generator, an in-house program at DLR Institute of Aeroelasticity
MTOM:	maximum take-off mass
MZFM:	maximum zero fuel mass
OEM:	operating empty mass
SOL101:	MSC.Nastran solver for static loads analysis
SOL144:	MSC.Nastran solver for static aeroelastic simulations
SOL146:	MSC.Nastran solver for dynamic aeroelastic simulations
SOL200:	MSC.Nastran solver for structure design and optimization
VTP:	vertical tailplane

* Research Associate, Loads Analysis and Aeroelastic Design
† PhD Candidate, Aerospace Structures and Materials
‡ Associate Professor, Aerospace Structures and Materials

I. Introduction

THE determination of loads acting on the aircraft is one of the main tasks during aircraft development since the structural mass directly influenced by the loads. One of the most heavily loaded components on an aircraft is the wing, which is also the focus of this work. To reduce wing loads and with it the wing's structural mass, methods of passive and active loads alleviation have been researched in recent years. However, load analysis with loads alleviation methods in the optimization process of aircraft predesign have not been carried out with a direct comparison between aluminum and composite aircraft. To consider all mentioned aspects, a loads and optimization process chain featuring dynamic simulations, unsteady aerodynamics and loads alleviation methods has been set up.

In the passive loads alleviation method, the material and stiffness properties of the wing are modified in a way that gust encounters or maneuvers evoke lower structural loads[1]. In the active loads alleviation method, additional functions are assigned to available control surfaces to redistribute lift during maneuvers and compensate lift increments during gust encounters to mitigate the structural loads[2,3,4]. In this work, the influence of both loads alleviation methods on the structural mass is to be investigated on a Generic Mid-Range (GMR) aircraft configuration. GMR is an aircraft configuration designed for approx. 150 passengers with a cruise Mach number of 0.78 and its mission profile is comparable with that of Airbus A320.

To perform this optimization, a gradient-based approach is preferred as the number of design variables is relatively large (approx. 600). However, the computation of required sensitivity over a transient response is not an easy task[5]. The equivalent static loads (ESL) method formalized by Kang et al.[6] is used to bypass this issue and provides optimized results for static and dynamic load cases.

II. Aircraft models

For the loads analysis of the aircraft, simulation models are built with ModGen[7]. ModGen is an in-house program at DLR Institute of Aeroelasticity, which is used to set up models for the loads analysis and the structural optimization. An overview of the aircraft parameters of the GMR configuration is shown in Table 1.

Table 1. Overview of aircraft parameter of the GMR configuration

Parameter	**Value**
Wing surface	122.3 m²
Wingspan	33.91 m
Mean aerodynamic chord	4.19 m
Operating Empty Mass	40638 kg
Maximum Zero Fuel Mass	60562 kg
Maximum Takeoff Mass	72545 kg
Maximum operating speed/Mach number	180 m/s EAS, Mach 0.82
Service ceiling	13000 m

A. Structure and mass model

For the loads simulations, FE-models of the GMR configuration are set up. The wing box, HTP box and the control surfaces are modeled with shell elements, whereas the fuselage is modeled with beam elements. The engine is modeled as a mass point with an approximated inertia and connected with a rigid pylon model to the wing; its shell elements in Figure 1(a) are for illustrational purpose only. Since only symmetric maneuvers and gusts are considered in the simulations, the aircraft is reduced to a half model. The masses of the fuselage and the VTP are accordingly halved. The VTP structure is replaced by single mass with the corresponding inertia and connected with a rigid element to the fuselage.

The aluminum aircraft model is assumed to be made of Aluminum 2024. For the aircraft model with passive loads alleviation, a composite wing box is required. In this case, the wing box material is changed to IM6, a carbon-epoxy composite material[8].

For the loads analysis, the structure and mass models are condensed onto the load reference axis (LRA) nodes in order to reduce the computational cost, since for the intended simulations only global mass and stiffness properties are significant. In Figure 1(b) the load reference axis nodes are marked with light blue triangles, which can be found on the fuselage, wing, engine, HTP, VTP and control surfaces.

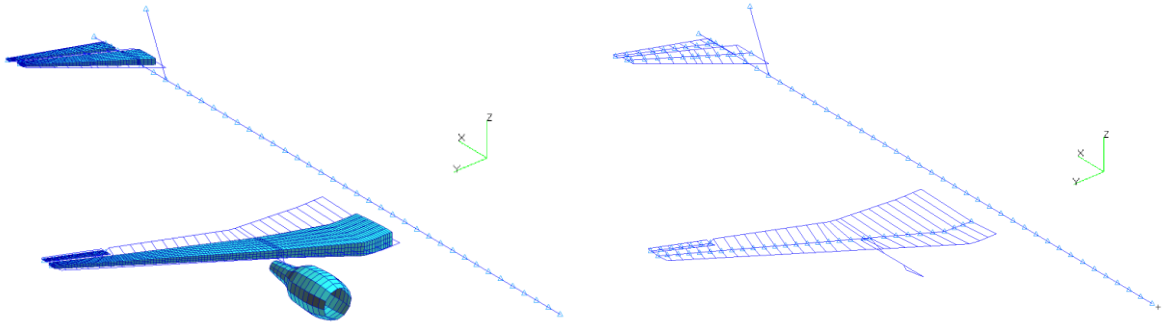

(a) (b)

Figure 1. Structural model of the Generic mid-Range configuration

B. Aerodynamic model

The aerodynamics is modeled with the Doublet-Lattice-Method (DLM) which is used in MSC.Nastran for gust analysis (SOL146) as well as the trim and maneuver analysis (SOL144). The wing and the empennage including their control surfaces are modeled with DLM boxes, while the fuselage is considered as a slender body element with its corresponding interference body, as shown in Figure 2(a) and (b). The displacement effect of the fuselage is created by the slender body element, whereas the evaluation of the downwashes is carried out on the interference body which is a cylinder with a constant radius circumscribing the slender body[9]. Although the slender body element in Figure 2(a) has a full circular cross section, in MSC.Nastran it is considered as a half body which is symmetric to the xz-plane. For the loads analysis, no aerodynamic correction such as twist or camber is taken into account.

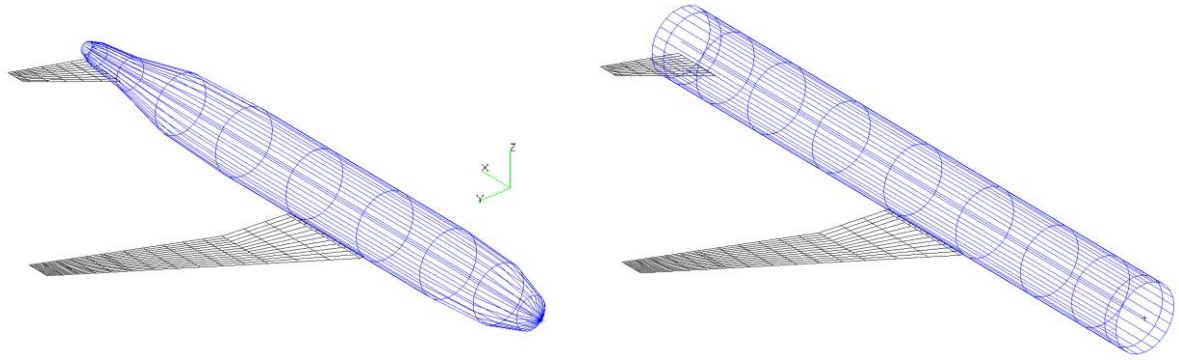

(a) (b)

Figure 2. Aerodynamic model of the Generic mid-Range configuration

C. Control surface model

For the aileron and elevator, the structure models are created with ModGen whereas typical wing box components such as upper and lower skin, spars and ribs are considered. The material thickness is adjusted to match the estimated masses according to Torenbeek[10]. The hinge between the control surface and the wing or empennage structure is modeled with bar elements. For loads analysis with the passive aircraft, a stiff torsion spring (10^7 Nm/rad) is set for the hinge. The FE-model of an aileron is shown in Figure 3. The bar elements which connects the aileron with the wing is drawn with thick blue lines. Figure 4 illustrates the aileron connection using bar elements and a torsion spring.

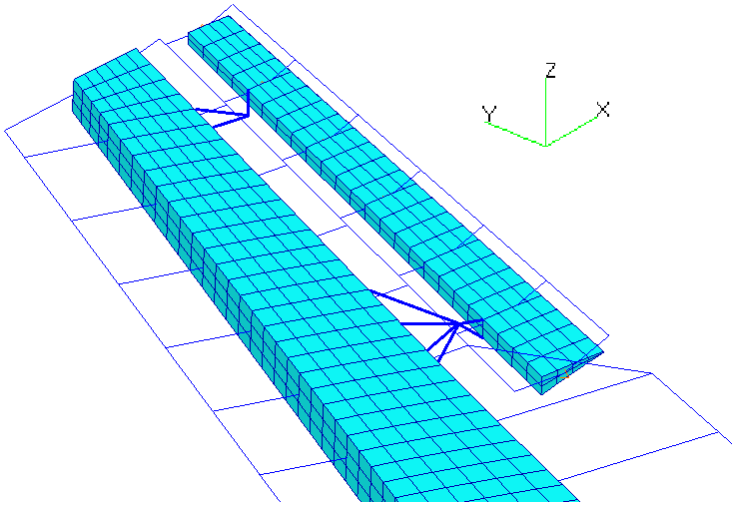

Figure 3. FE-Model of the aileron

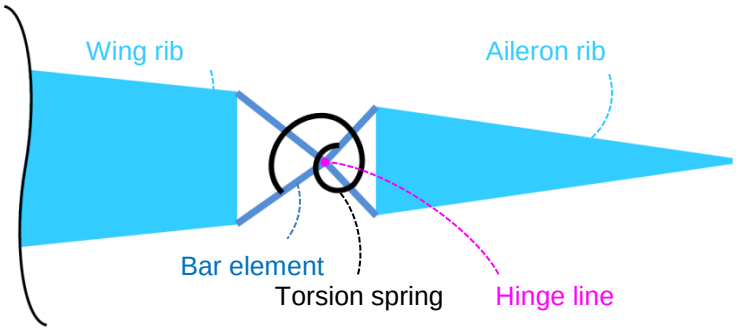

Figure 4. Illustration of the aileron connection

III. Loads and optimization process chain

To investigate the influence of the active and passive loads alleviation methods on the aircraft mass, a process chain is set up in MATLAB, whereas the loads analysis and structure optimization tasks are carried out with MSC.Nastran. A flowchart of the process chain is shown in Figure 5. In the first step, the stiffness and mass matrices of the condensed model are generated using the initial structural properties, whereas in the following steps the resulting design from the structure optimization is taken.

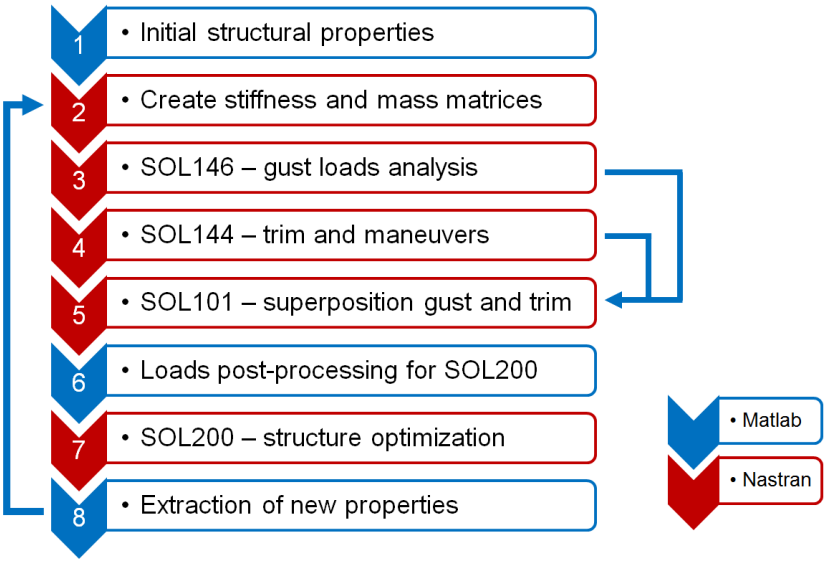

Figure 5. Process chain of loads analysis and structure optimization

A. Loads analysis

The loads analysis comprises symmetric maneuvers, trim as well as dynamic gust simulations according to CS25[11]. The quasi-steady maneuvers and the 1g trim calculations are carried out with SOL144, whereas SOL146 is used for the 1-cos-gust simulations in the frequency domain. In the dynamic simulations, a structural damping of 3% is assumed.

For the load case definition, four mass configurations and two flight conditions are considered. For each combination of mass configurations and flight conditions, one pull-up and one push-down maneuver are defined. This results in a total of 16 maneuvers. In the gust loads analysis, seven gust gradients are defined for every flight condition. The gust profiles are visualized in Figure 6. The gusts taken into account are vertical upward and vertical downward. In combination with the mass configurations, in total 104 gust cases are considered. The overview of the parameter space is presented in Table 2.

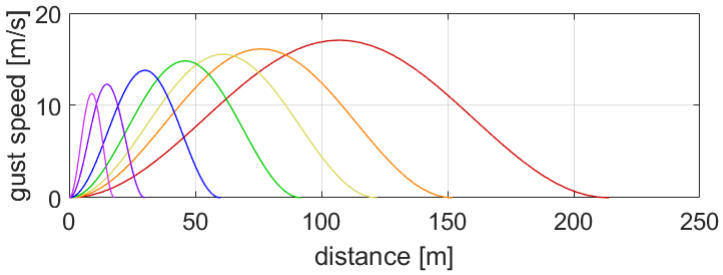

Figure 6. Overview of the 1-cos gust profiles taken into account

Table 2. Overview of parameter space of load simulations

Parameter	**Number**	**Remarks**
Mass configurations	4	MTOW (3 different centers of gravity) OWE
Flight conditions	2	V_C at sea level and 7000 m
Gust gradients	7	9 - 107 m
Gust directions	2	Vertical upward and downward
Maneuvers	2	Symmetric 2.5g and -1g maneuvers
Trim	1	Steady 1g trim
Total number of gust cases	**104**	Combination of mass configurations, flight conditions, gust gradients, gust directions
Total number of maneuver cases	**16**	Combination of mass configurations, flight conditions, maneuvers

B. Loads post-processing

For the quasi-steady maneuvers, each maneuver case delivers a set of nodal loads. With a total of 16 considered maneuver cases, accordingly 16 sets of nodal loads are generated. In the dynamic gust simulations however, the results can be printed as time histories of loads, from which design loads for the structure optimization have to be extracted. For this purpose, two filtering steps are implemented. At first, six cut load monitoring points are created on the wing, as shown in Figure 7. In every gust simulation, each time the shear force, bending moment or torque of each monitoring point reaches its maximum or minimum as depicted in Figure 8, all nodal loads and cut loads are extracted. This is the first step of the filtering. Since in SOL146 only incremental gust loads are considered, the extracted nodal loads and cut loads have to be superposed with those from the corresponding trim calculations to obtain the total loads.

In the second step of filtering, for the superposed cut loads from the gust simulations and maneuver loads, 2D envelopes are determined from the cut load combinations M_x/M_y, as shown in Figure 9, as well as M_x/F_z. This method is applied to every monitoring station. The load cases appearing on the 2D envelopes comprise the loads considered in the structure optimization.

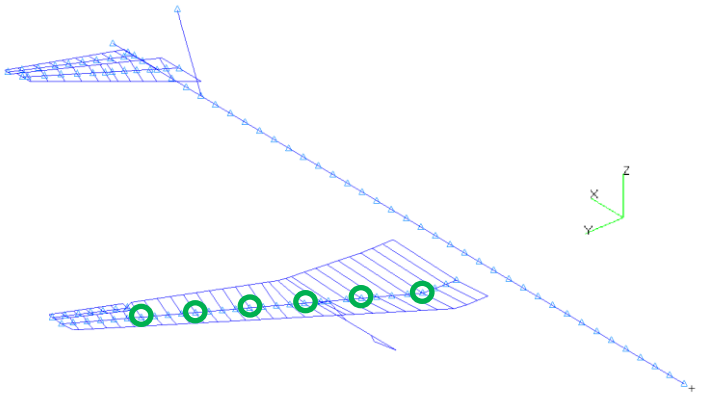

Figure 7. Monitoring points on the wing

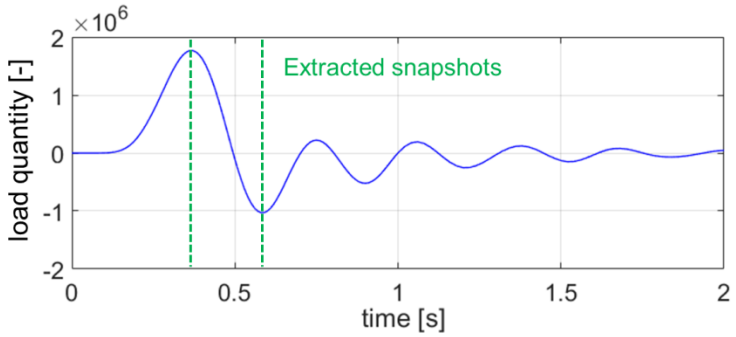

Figure 8. Extracted snapshots of a gust simulation

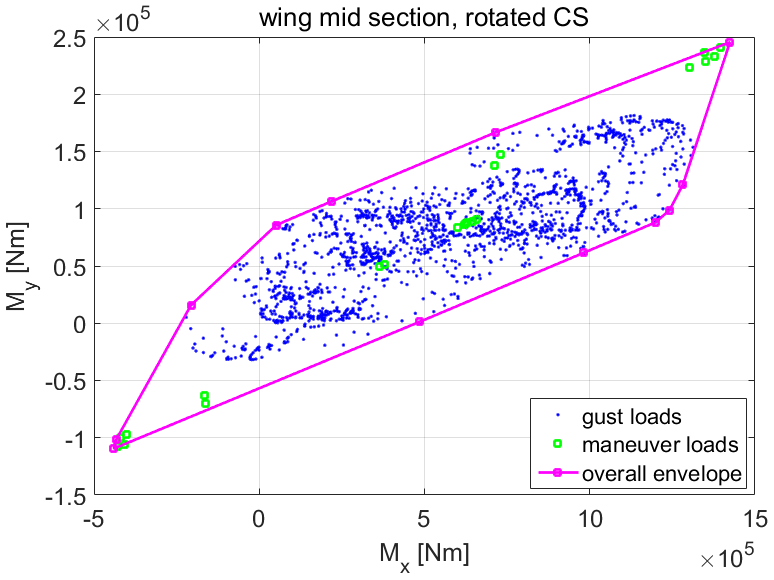

Figure 9. Convex hull surrounding gust and maneuver loads

C. Structure optimization

For the structure optimization, 66 design fields are defined for the wing box. These consist of 22 fields for each the upper and lower skin, each 11 fields for the front and rear spar. The number of the design fields results from a compromise between the detail level of the material thickness distribution and computation time-saving in the structure optimization. The 22 design fields on the upper skin of the wing are shown in Figure 10. The filtered nodal loads from the loads analysis are then input into SOL200, the structure optimization module of MSC.Nastran. The objective is to minimize the wing box mass. The constraints considered in the structure optimization process are buckling and von-Mises stress for the aluminum aircraft, respectively the first layer failure criterion for the composite aircraft. The buckling constraint is based on the approach by Klimmek[5] with a uniaxial loaded plate strip, where the stringer pitch is assumed as the buckling field width. However, in the GMR FE-model the stringer

pitch varies along the half span due to the taper ratio and because the number of stringers is constant. To avoid having very large buckling field widths in the wing root area, a constant stringer pitch of 250 mm is assumed in the buckling stress calculation for the whole wing box.

The minimum aluminum thickness allowed in the optimization is 2 mm, while the composite laminate thickness has to be at least 4 mm. An overview of the objective and constraints is presented in Table 3.

To create the initial thickness distribution, the wing box is optimized with loads from one pull-up maneuver at the maximum take-off mass using a rigid model. For the composite aircraft, the initial thickness distribution from the aluminum model is taken and multiplied by 1.5, since composite wing boxes tend to have larger material thicknesses compared to aluminum. Besides, all lamination parameters are set to zero, which makes the initial composite laminate a quasi-isotropic material.

Table 3. Overview of optimization parameters

Parameter	Number	Remarks
Skin design fields	44	22 upper skin, 22 lower skin design fields
Spar design fields	22	11 front spar, 11 rear spar design fields
Objective	1	Minimum mass
Constraints (aluminum aircraft)	132 66	Von-Mises stress at both shell sides Buckling
Constraints (composite aircraft)	4176 66 66	First layer failure on both shell sides Lamination parameter compatibility Buckling

In order to achieve an optimized design, five cycles consisting of loads analysis and subsequent structure optimization are considered as sufficient. This method has the advantage to be easy to implement regardless of the different tools used in the loop. For example, it can be extended already existing gradient-based optimization and aeroelastic analysis code and was already applied to similar aerostructural problems where gust loads are introduced in the optimization[12].

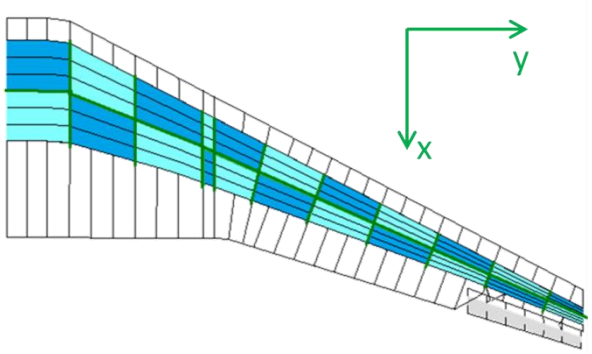

Figure 10. 22 design fields on the upper skin of the wing

IV. Passive loads alleviation

The passive loads alleviation is implemented with aeroelastic tailoring. The design variables used here are the panel thickness and the laminations parameters. This formulation has been first introduced by Tsai et al.[13] and is used as a representation of the [A, B, D] stiffness matrix from the classical lamination theory. As the optimization is done for both the in-plane and out-of-plane responses, only eight laminations parameters per panel are necessary to fully describe any symmetrical stacking sequences. Laminations parameters present the advantage to be continuous compared to discrete ply angles. This continuous formulation greatly helps the optimizer to perform its task but does not directly define a proper stacking sequence. This is usually done as a post-processing step using a genetic algorithm, but is not achieved in the present work. Thus, with eight lamination parameter and skin thickness, there are nine optimization variables in each design field, which makes a total of 594 variables for the GMR wing box with 66 design fields.

Using a continuous formulation also requires using appropriate constraints for the maximum allowable strain. As the fibers orientations remain unknown, it is impossible to properly predict the actual failure envelope of a stacking sequence solely defines by its stiffness property. IJsselmuiden et al.[8] proposed a formulation of the widely used Tsai-Wu failure criteria for the continuous optimization, by defining the area of the failure envelope common to the entire ply angles.

V. Active loads alleviation

A. Maneuver Loads alleviation

For the quasi-steady maneuver simulations, Maneuver Loads alleviation (MLA) is implemented by deflecting the ailerons symmetrically, 10° upward for the pull-up maneuvers and 10° downward for the push-down maneuvers. The value of 10° is a conservative assumption based on the MLA implemented on the L-1011 Tristar[14] with an actuation limit of 13°. Figure 11 shows the desired effect of MLA by changing the lift distribution on the wing, with it a smaller wing bending moment can be achieved at the same total lift force.

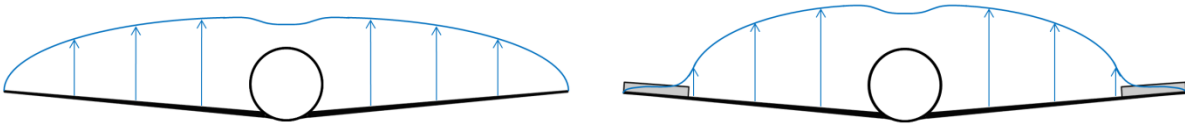

Figure 11. Change of lift distribution due to MLA

B. Gust Loads alleviation

For the Gust Loads alleviation (GLA), a feed-forward controller is implemented. The controller is defined to react to the angle of attack increment due to gust and deflect the ailerons symmetrically. It is assumed that the angle of attack is measured at the aircraft nose and the calculation of the gust induced angle of attack has been derived by König et al.[15]. To simplify the approach, a proportional controller is chosen. Additionally, a delay time and a low pass are also considered. The block diagram of the control system is presented in Figure 12. Besides, since the short period motion due to gusts does not evoke maximum loads, the deflection of the elevators to control the pitch is not considered as necessary.

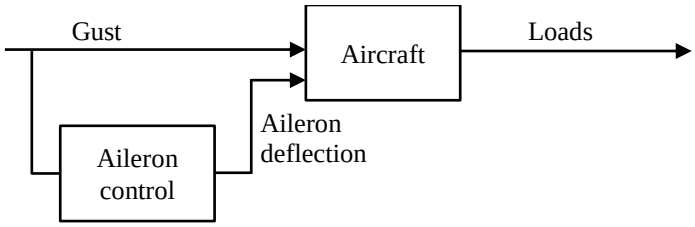

Figure 12. Block diagram of the active loads alleviation system

The amplitude of the proportional controller is set to 1.5. It means that with an angle of attack increment of 1° the aileron will deflect 1.5°. This value is chosen as a compromise between the deflection rate limitation and the compensation of lift due to gust on the outer part of the wing by aileron deflection, whereas the aileron aerodynamic efficiency is set to 0.7. The aerodynamic efficiency implies the ratio between the actual force induced by aileron deflection and the ideal solution of two-dimensional potential theory. As a reference: according to the potential theory described by Schlichting-Truckenbrodt[16], with a chord ratio of the control surface of 0.33 and its efficiency of 0.75, a proportionality factor of 1.67 would be necessary to compensate lift due to gust with aileron deflection.

The delay time is set to a standard value of 80 ms. It is intended to simulate the data acquisition and computation delay of the Flight Control System of the aircraft. Besides, 80 ms is approximately the time between the gust detection at the aircraft nose and the gust encounter of the wing at the sizing relevant flight condition. According to Wildschek[3], the delay time of such control system must not be greater than 100 ms to ensure that the controller is causal for all load cases. In his work, a delay time of 60 ms is assumed. For the controller, a two-pole low pass is set at 4 Hz. The low pass is supposed to limit the aileron actuation rate during short gust encounters to slightly below 40°/s since no other rate limiter is implemented. Figure 13 shows the resulting aileron travel rates for different gust gradients after implementing the low pass. As a comparison, the amplitude ratios between the different gust gradients can be seen in Figure 6.

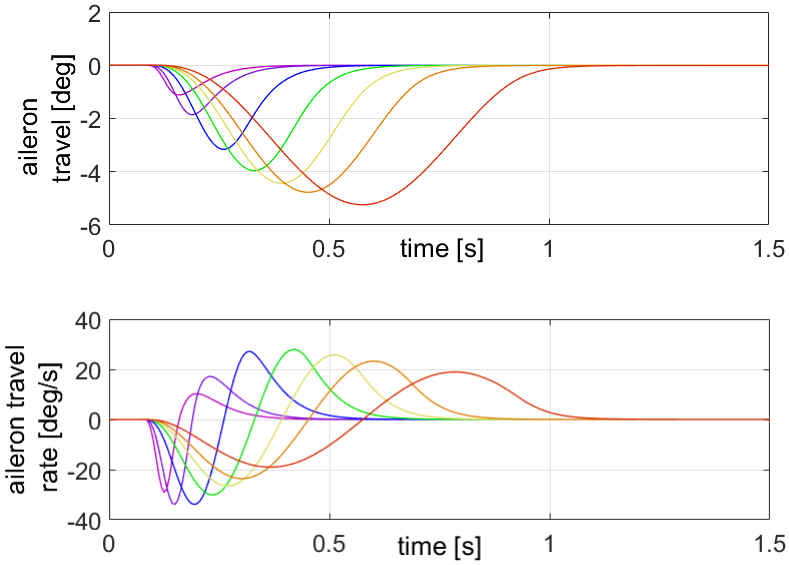

Figure 13. Time history of aileron travel and travel rate for different gust gradients

VI. Results

A. Comparison of wing box masses

The cycles of loads analysis and structure optimization are applied to the aluminum and composite aircraft model, with and without active control each. The comparison of the aircraft masses after four cycles is presented in Table 4. The biggest decrease in wing box mass is achieved by using composite materials. However, an aspect to pay attention for is that in this direct comparison both aluminum and composite aircraft models have the same number of design fields. If manufacturing aspects are taken into account, the aluminum aircraft can have a significantly larger number of design fields due to the easier processing of aluminum. In that case, a design field can be as small as the area between two ribs and two stringers and the thickness distribution can be optimized in a finer way, which would lead to a further mass reduction. An example of a convergence history is shown in Figure 14. Between the last two iterations the wing box mass of the passive aluminum aircraft changed by 32 kg or 0.7%.

Table 4. Overview of wing box mass comparison

Aircraft model	Wing box mass [kg]	Relative difference [%]
Passive, aluminum	4438.	0.0%
Active, aluminum	4293.	-3.3%
Passive, composite	3515.	-20.8%
Active, composite	3421.	-22.9%

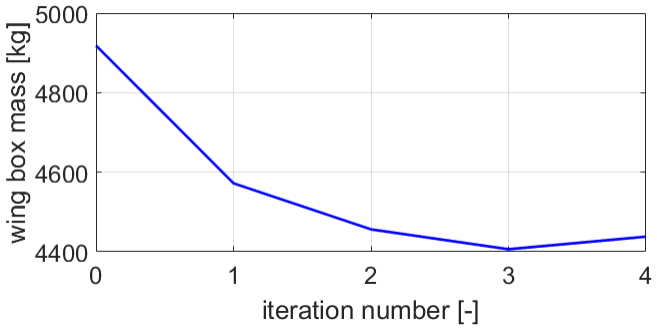

Figure 14. Convergence history of the passive aluminum aircraft

B. Comparison of loads envelopes

From the four investigated aircraft designs, a comparison of 2D loads envelopes of the bending moment M_x and torsion M_y at the wing middle section is shown in Figure 15. It is apparent that the loads envelopes of both passive aircraft overlap almost perfectly, and the same also applies to both active aircraft, whereas the envelopes of the composite aircraft tend to be more slender. In this kind of visualization, the implementation of the loads alleviation methods causes a counterclockwise rotation of the envelopes, which means a lower maximum bending moment M_x but a slightly higher torsion M_y. Thereby, the magnitude of the rotation depends on the amplitude of the loads alleviation systems. At the middle wing section the bending moment is reduced by around 14% and the torsion increases by 8%.

Towards the wing root, the rotation of the envelopes is expected to be less pronounced since the percentage of lift and moment change due to loads alleviation methods is less compared to the wing middle section or the wing tip. Besides, the engine inertia has a significant contribution to the torsion due to gusts, and this surpasses the torsion due to maneuvers. A comparison of the loads envelopes at the wing root is shown in Figure 16. The maximum torsion M_y due to gusts occurs where the bending moment M_x is at about 10^6 Nm, whereas the maximum and minimum bending moment M_x still occur during maneuvers. Thereby, a bending moment reduction of 8% can be achieved with loads alleviation. In the torsion M_y, both composite aircraft have lower maximum values of up to 24% compared to both aluminum aircraft.

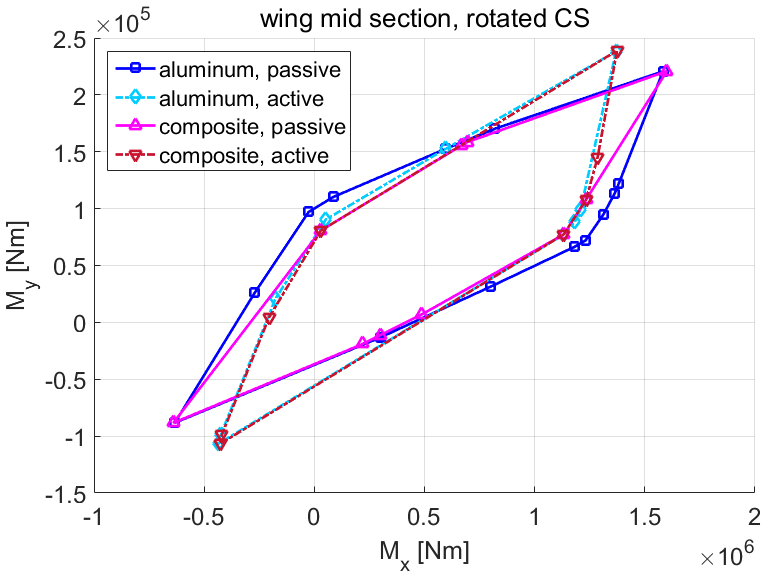

Figure 15. Comparison of 2D loads envelopes at the wing middle section

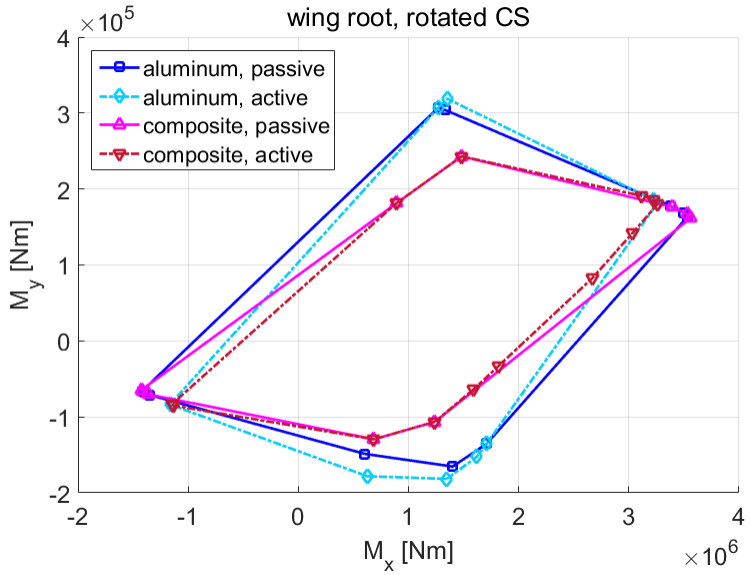

Figure 16. Comparison of 2D loads envelopes at the wing root

C. Structural comparison between active and passive aluminum aircraft

Compared to the passive aluminum model, a reduction of the wing box mass by 145 kg or 3.3% is achieved with active loads alleviation. If referred to the operating empty mass (OEM), this equals to a reduction by 0.4%. However, a decrease in the wing box mass would also evoke a decrease in other components such as fuselage structure as well, which would result in a higher overall mass reduction. The wing box skin thicknesses of the passive and active aircraft are presented in Figure 17 and Figure 18. It is apparent that the skin of the passive aircraft is thicker in general; the orange and yellow areas on the upper skin as well as the green ones on the lower skin extend further towards the wing tip.

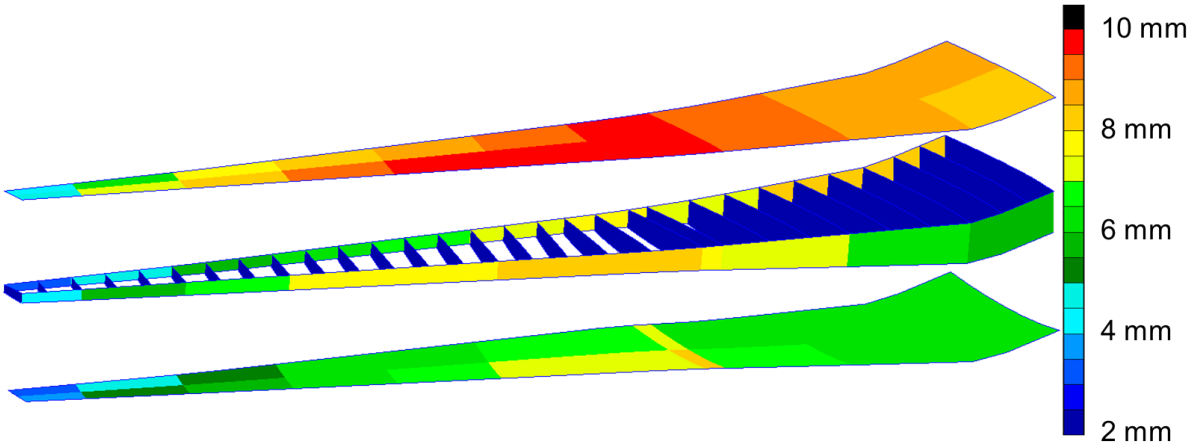

Figure 17. Wing box thickness distribution of the passive aluminum aircraft

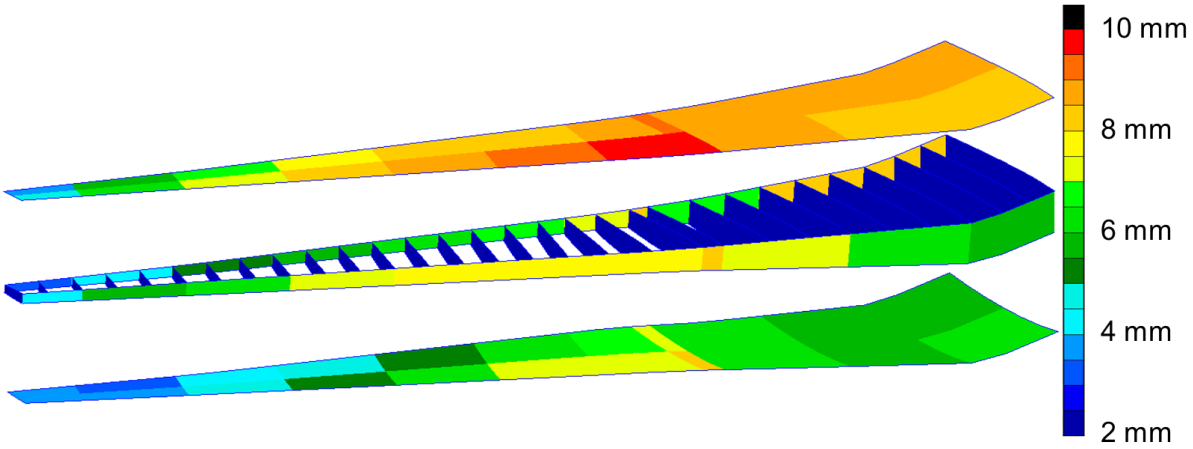

Figure 18. Wing box thickness distribution of the active aluminum aircraft

D. Structural comparison between active and passive composite aircraft

On the active composite aircraft, the implementation of loads alleviation methods yields a mass decrease of 94 kg or 2.7% compared to the wing box of the passive composite aircraft. Concerning the skin thickness distributions as shown in Figure 19 and Figure 20, almost every design field on the lower skin of the active aircraft has a lower thickness, while on the upper skin the root area of the active aircraft is slightly thicker. To get a deeper insight into the stiffness distributions, stiffness curves – directional tensile moduli multiplied with the thickness – of a few selected skin design fields are visualized in Figure 21. On the upper skin, the stiffness curves of both active and passive aircraft are almost identical, except at the outer part near the front spar, where the active aircraft is around 32% softer in the spanwise direction. Regarding the lower skin at the root, the active aircraft has 17% less spanwise stiffness in the rear half. At the wing outer part, the front half on the active aircraft is around 23% softer in the spanwise direction. Furthermore, judging by the size of the stiffness curves, the upper skin has a larger in plane stiffness compared to the lower skin, which is also the case on the aluminum aircraft.

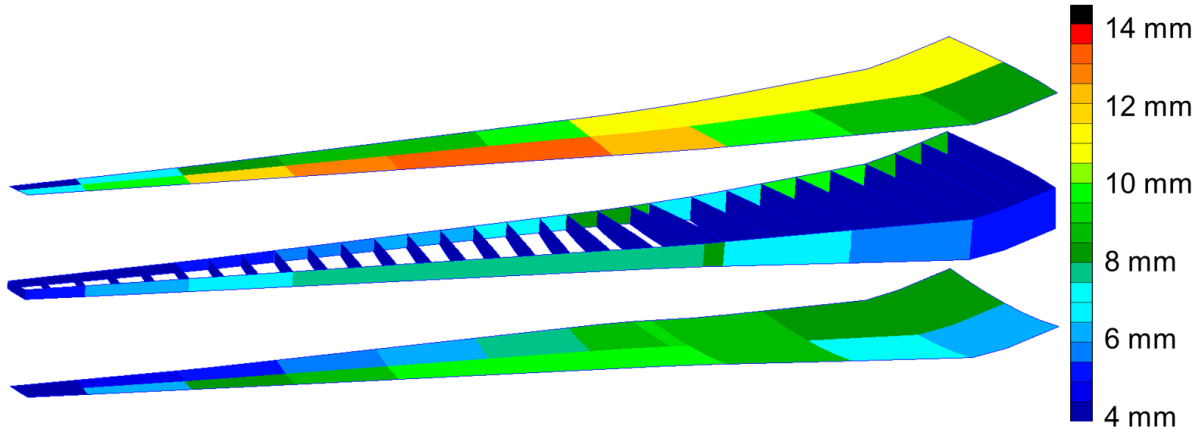

Figure 19. Wing box thickness distribution of the passive composite aircraft

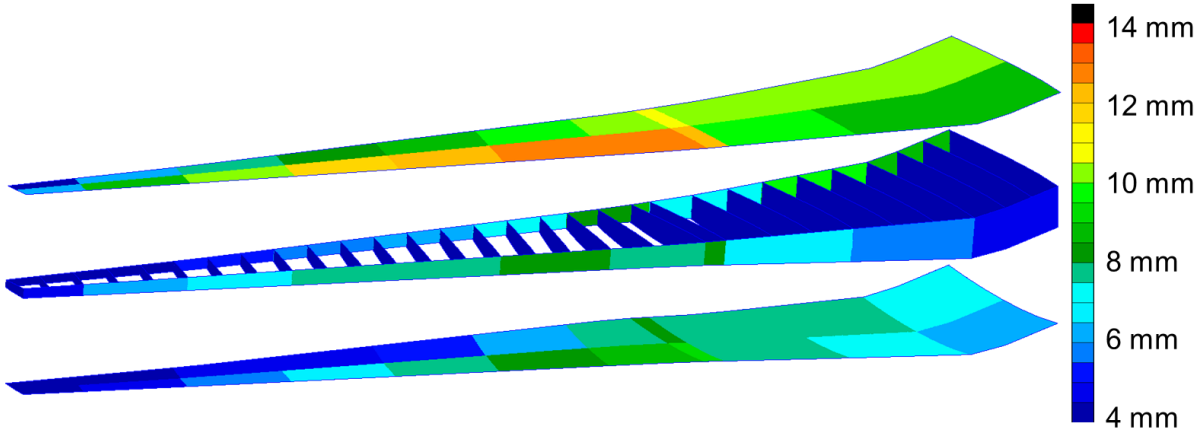

Figure 20. Wing box thickness distribution of the active composite aircraft

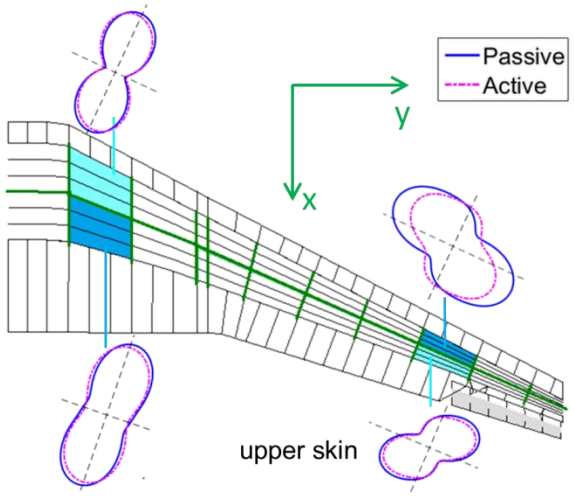

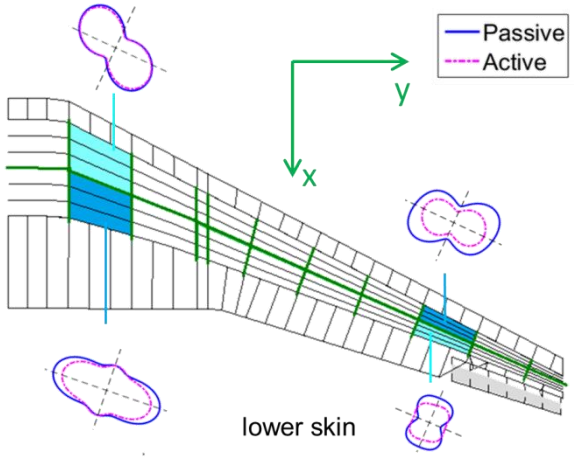

(a) (b)

Figure 21. Stiffness curves of selected design field on the upper skin (a) and lower skin (b)

E. Aileron effectiveness

According to CS25[11], no control reversal may occur at any speed up to 1.15 of the design dive speed V_D. If the torsional stiffness of an aircraft wing becomes softer than the initial design due to loads alleviation, the airspeed or dynamic pressure at which control reversal occurs can decrease. For this reason, a check of the aileron reversal is necessary. This is conducted by monitoring the aircraft's aileron derivatives at $1.15 \cdot V_D$ at sea level – at Mach 0.693 and with a dynamic pressure of 34,090 Pa.

Since the half model of GMR only allows symmetric motions, the monitored derivative is lift increment for the whole aircraft c_z due to aileron deflection ξ, defined as $c_{z\xi}$. Thereby, the derivative of the elastic aircraft $c_{z\xi}$(elastic) is compared to that of the rigid aircraft $c_{z\xi}$(rigid) and this ratio is defined as aileron effectiveness. Aileron reversal is assumed not to occur if the aileron effectiveness is positive:

$$\left.\frac{c_{z\xi}(\text{elastic})}{c_{z\xi}(\text{rigid})}\right|_{1.15 \cdot V_D} > 0 \qquad (1)$$

An aspect to remark is that this is a conservative approach, since with a total vertical force of zero – which would mean zero aileron effectiveness according to equation (1) – the aircraft still can roll. This can occur for example if the total lift in the wing outer part – due to aileron deflection and elastic twist – is equal to the downforce magnitude in the wing inner part due to elastic twist.

The aileron effectiveness of each aircraft model at $1.15 \cdot V_D$ is listed in Table 5. Since all values are positive, aileron reversal does not occur on any of the aircraft models since the dynamic pressure of 34090 Pa will not be exceeded in the rest of the prescribed flight envelope.

Table 5. Overview aileron effectiveness at 1.15 of design dive speed V_D

Aircraft model	Aluminum		Composite	
	Passive	Active	Passive	Active
Aileron effectiveness	9.4%	6.0%	14.9%	10.3%

F. Parameter study: Variation of GLA delay time

The influence of GLA delay time on the loads envelope has been investigated on one maximum take-off mass configuration. A variation of the delay time between 60 and 100 ms is taken into account. As a comparison: the time shift between the gust at the nose sensor and at the aileron position varies between 80 and 110 ms, depending on the airspeed. However, since the feed-forward controller has a low pass at 4 Hz, there is an additional phase shift due to the low pass which delays high-frequency deflections further. In the bending moment M_x, the incremental gust loads with a GLA delay of 100 ms are up to 7.5% larger compared to those with 60 ms delay. On the other hand, the torsion M_y is not affected by the change in delay time. This occurrence implies that a decrease of GLA delay time leads to a larger reduction of the wing bending moment M_x.

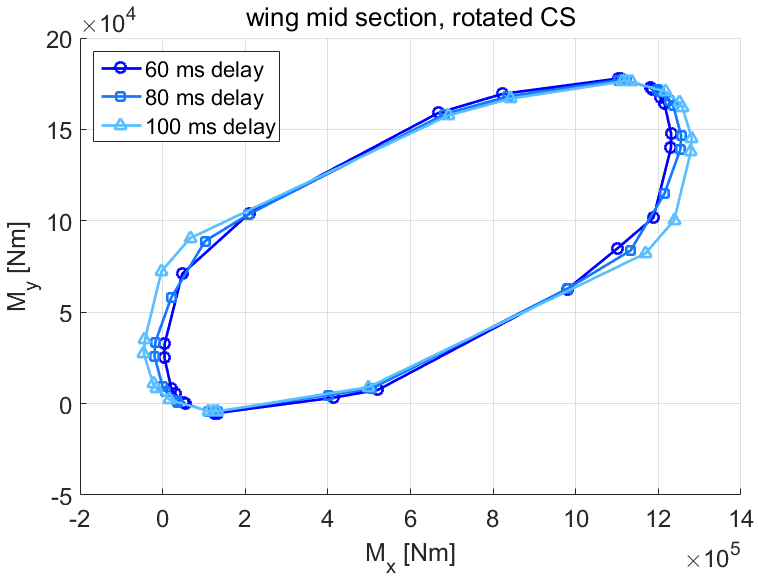

Figure 22. Change in gust load envelope due to delay time variation

VII. Conclusion and outlook

The implementation of an active and passive loads alleviation method on a generic mid-range aircraft configuration has been presented. For the active loads alleviation, methods to reduce both maneuver and gust loads have been implemented. The maneuver loads alleviation is implemented by defining a symmetric aileron deflection during pull-up and push-down maneuvers, while the gust loads alleviation is a feed-forward system reacting to the incremental angle of attack due to gust. The passive loads alleviation is carried out by changing the wing box stiffness properties using composite material and variable lamination parameters in the structure optimization. With the combination of actively controlled/passive aircraft and aluminum/composite wing box, in total four aircraft models have been investigated. In the entire process, four cycles of loads analysis and subsequent structure optimization have been carried out for all four aircraft.

The results show that the implemented active loads alleviation system can reduce the wing root bending moment by 8%, which result in a wing box mass decrease by 2.7% to 3.3%. On the other hand, the implemented passive loads alleviation can help in reducing the root torsion by 24% and the wing box mass by around 21%. However, this value results from the identical boundary conditions for both aluminum and composite aircraft, in terms of the same number of design fields. In reality, an aluminum wing can be discretized into smaller design fields resulting in a more optimized thickness distribution and a lower structural mass.

In the modeling aspect, an advisable extension to the aerodynamic model is an addition of DLM boxes for the engine nacelles, since these would provide aerodynamic damping in dynamic simulations and reduce the wing root torsion.

A possible process extension for the future is the inclusion of rib properties as variables and with it also the structural constraints in the ribs. To define the design fields, it is advisable to divide the ribs into the same number of design fields as the skins and spars along the half span, in this case eleven. This is intended to avoid having ribs from the same design field connected to components from too many other design fields, since this might increase the size of the optimization process or lead to convergence problems. An exemplary extreme case to be avoided is assigning all ribs to one single design field, since a change of rib properties would impact the stiffness on the whole wing box, and with it practically all other design fields are affected.

A further possible approach is to investigate the fatigue behavior of both active and passive aircraft. For this purpose a typical mission scenario can be simulated, including typical turbulences encountered in the respective flight phases. The GLA described in this work can also be retrofitted with an additional wing bending damper[17] to reduce the number of structure oscillation cycles in turbulent air and with it extend the fatigue life.

Acknowledgments

The author (V. Handojo) thanks the colleagues from the department Aerospace Structures and Materials, Faculty of Aerospace Engineering, Delft University of Technology for the hospitality during the research on the described topic in Spring 2017.

References

[1] Dillinger, J. (2014). Static Aeroelastic Optimization of Composite Wings with Variable Stiffness Laminates. Delft: Delft University of Technology.

[2] Teufel, P. (2003). Böenmodellierung und Lastabminderung für ein flexibles Flugzeug. Stuttgart: Universität Stuttgart.

[3] Wildschek, A. (2008). An Adaptive Feed-Forward Controller for Active Wing Bending Vibration Alleviation on Large Transport Aircraft. München: Technische Universität München.

[4] Xu, J. (2012). Aircraft Design with Active Load Alleviation and Natural Laminar Flow. Stanford: Stanford University.

[5] Bettebghor, D. and Blondeau, C. (2013). "Prise en compte de la flexibilité des cas de charges dimensionnants en optimisation de structure", in proceeding of 11e Colloque National en Calcul des Structures, Giens.

[6] Kang, B. S., Choi, W. S. & Park, G. J. (2001). "Structural optimization under equivalent static loads transformed from dynamic loads based on displacement", Comput. Struct. 79, pp. 145–154.

[7] Klimmek, T. (2009). Parameterization of topology and geometry for the multidisciplinary optimization of wing structures, in *CEAS - European Air and Space Conference*, Manchester, United Kingdom.

[8] IJsselmuiden, S.T., Abdalla, M.M. and Gürdal, Z. (2008). "Implementation of strength based failure criteria in the lamination parameter design space", AIAA J. 46, pp. 1826–1834.

[9] MSC.Software Corporation (2004). "MSC.Nastran Version 68 – Aeroelastic Analysis User's Guide, " MSC.Software.

[10] Torenbeek, E. (1992). "Development and Application of a Comprehensive, Design-sensitive Mass Prediction Method for Wing Structures of Transport Category Aircraft, " TU Delft, Delft.

[11] European Aviation Safety Agency (2015). Certification Specifications and Acceptable Means of Compliance for Large Aeroplanes CS-25, Amendment 16.

[12]Kim, Y.I., Park, G.J., Kolonay, R.M., Blair, M. and Canfield, R.A. (2009). "Nonlinear Dynamic Response Structural Optimization of a Joined-Wing Using Equivalent Static Loads", J. Aircr. 46, pp. 821–831.

[13]Tsai, S.W. and Pagano, N.J. (1968). "Invariant properties of composite materials", Def. Tech. Inf. Cent.

[14]Ramsey, H.D. and Lewolt, J.G. (1979). "Design Maneuver Loads for an Airplane with Active Control System," Structures, Structural Dynamics, and Materials Conference, 20th, St. Louis, Mo.

[15]König, R; Hahn, K.U. (1990). "Load Alleviation and Ride Smoothing Investigations Using ATTAS," Proceedings of the 17th ICAS.

[16]Schlichting, H., & Truckenbrodt, E. (1969). Aerodynamik des Flugzeuges, Band 2. Berlin, Heidelberg, New York: Springer-Verlag.

[17]P. Burris and M. Bender (1969). "Aircraft Load Alleviation and Mode Stabilization," Air Force Flight Dynamics Laboratory, Wright-Patterson Air Force Base, Ohio.